J|A|C|S ARTICLES

Published on Web 02/11/2009

Characterization of Fluorescence in Heat-Treated Silver-Exchanged Zeolites

Gert De Cremer,[†] Eduardo Coutiño-Gonzalez,[‡] Maarten B. J. Roeffaers,[‡] Bart Moens,[†] Jeroen Ollevier,[‡] Mark Van der Auweraer,[‡] Robert Schoonheydt,[†] Pierre A. Jacobs,[†] Frans C. De Schryver,[‡] Johan Hofkens,[‡] Dirk E. De Vos,[†] Bert F. Sels,*[,†] and Tom Vosch*[,‡]

Department of Microbial and Molecular Systems, Centre for Surface Chemistry and Catalysis, Katholieke Universiteit Leuven, Kasteelpark Arenberg 23, B-3001 Leuven, Belgium, and Department of Chemistry, Katholieke Universiteit Leuven, Celestijnenlaan 200F, B-3001, Leuven, Belgium

Received December 26, 2008; E-mail: bert.sels@biw.kuleuven.be; tom.vosch@chem.kuleuven.be

Abstract: Thermal treatment of Ag^+-exchanged zeolites yields discrete highly photostable luminescent clusters without formation of metallic nanoparticles. Different types of emitters with characteristic luminescence colors are observed, depending on the nature of the cocation, the amount of exchanged silver, and the host topology. The dominant emission bands in LTA samples are situated around 550 and 690 nm for the samples with, respectively, low and high silver content, while in FAU-type materials only a broad band around 550 nm is observed, regardless of the degree of exchange. Analysis of the fluorescent properties in combination with ESR spectroscopy suggests that a Ag_6^+ cluster with doublet electronic ground state is associated with the appearance of the 690-nm emitter, having a decay of a few hundred microseconds. Tentatively, the nanosecond-decaying 550-nm emitter is assigned to the Ag_3^+ cluster. This new class of photostable luminescent particles with tunable emission colors offers interesting perspectives for various applications such as biocompatible labels for intracellular imaging.

Introduction

The peculiar optical properties of small metal clusters are an intriguing research topic for physical chemists. In contrast to bulk metals, small oligoatomic metal clusters (M_n^{m+} with $n < 100$ and $m < n$) are known to have discrete electronic energy states, and thus have a molecule-like behavior with respect to electronic transitions. For specific cluster types of noble metals such as gold and silver, bright emission upon excitation within the UV−visible range has been reported.[1−7] Cluster size and charge affect the emission color. The selective synthesis of such oligoatomic clusters is heavily complicated by the inevitable aggregation tendency of noble metal clusters, extinguishing the emissive properties. Throughout the years, many strategies have been explored to obtain defined oligoatomic metal clusters. For instance, mass-selected oligoatomic metal clusters can be cooled in a noble gas flow to cryogenic temperatures. Upon condensation, a stabilizing shell is formed around the clusters. This technique was already reported in the 1970s by Ozin and Huber[8] and has been used for systematic identification of fluorescence properties of small silver and gold clusters.[1,2] Ertl's group recently reported on chemiluminescence during silver condensation with argon. The light emission was explained by the formation of excited Ag_2* and Ag_3* clusters during the reaction.[5] As these extreme synthesis conditions are not amenable for applications, alternative stabilization protocols are required. The high coordination affinity of silver for the lone-pair electrons of, for example, nitrogen has been successfully exploited by using cytosine-rich DNA strands as a scaffold for small silver clusters.[3,4,7] Similarly, polyphosphates,[9,10] peptides,[11] or polymers such as poly(acrylic acid)[12] have been proposed as stabilizing agents preventing cluster agglomeration.

Recently, confinement strategies have been used to embed metal clusters in glass.[13] More particularly, the molecularly sized cages of zeolites are perfectly suited to accommodate oligoatomic metal clusters.[14−19] Zeolites are crystalline inorganic materials typically having a cation exchange capacity that

[†] Department of Microbial and Molecular Systems.
[‡] Department of Chemistry.

(1) Fedrigo, S.; Harbich, W.; Buttet, J. *J. Chem. Phys.* **1993**, *99*, 5712.
(2) Felix, C.; Sieber, C.; Harbich, W.; Buttet, J.; Rabin, I.; Schulze, W.; Ertl, G. *Chem. Phys. Lett.* **1999**, *313*, 105.
(3) Petty, J. T.; Zheng, J.; Hud, N. V.; Dickson, R. M. *J. Am. Chem. Soc.* **2004**, *126*, 5207.
(4) Richards, C. I.; Choi, S.; Hsiang, J. C.; Antoku, Y.; Vosch, T.; Bongiorno, A.; Tzeng, Y. L.; Dickson, R. M. *J. Am. Chem. Soc.* **2008**, *130*, 5038.
(5) Schulze, W.; Rabin, I.; Ertl, G. *ChemPhysChem* **2004**, *5*, 403.
(6) Treguer, M.; Rocco, F.; Lelong, G.; Le Nestour, A.; Cardinal, T.; Maali, A.; Lounis, B. *Solid State Sci.* **2005**, *7*, 812.
(7) Vosch, T.; Antoku, Y.; Hsiang, J. C.; Richards, C. I.; Gonzalez, J. I.; Dickson, R. M. *Proc. Natl. Acad. Sci. U.S.A.* **2007**, *104*, 12616.
(8) Ozin, G. A.; Huber, H. *Inorg. Chem.* **1978**, *17*, 155.
(9) Henglein, A. *Chem. Rev.* **1989**, *89*, 1861.
(10) Mulvaney, P.; Henglein, A. *J. Phys. Chem.* **1990**, *94*, 4182.
(11) Yu, J.; Patel, S. A.; Dickson, R. M. *Angew. Chem., Int. Ed.* **2007**, *46*, 2028.
(12) Keghouche, N.; Mostafavi, M.; Delcourt, M. O. *J. Chim. Phys. Phys.-Chim. Biol.* **1991**, *88*, 855.
(13) Karthikeyan, B. *J. Appl. Phys.* **2008**, 103.
(14) Baker, M. D.; Godber, J.; Ozin, G. A. *J. Phys. Chem.* **1985**, *89*, 2299.
(15) Jacobs, P. A.; Uytterhoeven, J. B. *J. Chem. Soc., Faraday Trans.* **1979**, *75*, 56.

facilitates the uptake and location of silver ion precursors within their pores and cages. A subsequent reduction step transforms the metal cations into oligoatomic clusters, the size of which is influenced by the dimensions of the zeolite cages. Moreover, the negative charge of the zeolite lattice and the coordinating properties of the lattice oxygen atoms provide an additional stabilization of (partially charged) metal clusters.

Silver-exchanged zeolites have been extensively studied since the 1970s because of their promising catalytic properties.[15,20,21] It was reported that, upon drying of these silver-containing zeolites, the color changed from white over yellow to brick red.[15,17,22,23] Dehydration of the silver ions has been suggested to induce this effect.[17,24−27] These highly colored ionic silver complexes, however, have poor fluorescent properties at room temperature.[25] Recently, we explored the emissive behavior of silver-exchanged zeolites after careful reduction with UV irradiation.[28] Highly emissive spots inside the zeolite particles have been observed at ambient conditions. Reduction of silver in zeolite hosts has been alternatively carried out by chemical agents such as hydrogen gas, CO, or sodium borohydride, but also γ-irradiation[29−31] and irradiation with visible light[32] induce reduction of silver ions with formation of (charged) silver clusters. In the particular case of silver zeolites, autoreduction processes have been recognized when the zeolites are exposed to a simple vacuum dehydration or heating treatment. The required electrons originate from the expulsion of oxygen atoms from the zeolite framework or from the oxidation of hydration water to oxygen.[15,21,26,27] Autoreduction is a practical method for preparing highly emissive and very photostable particles of use in a wide variety of applications such as biocompatible labels. This work studies thermally, (auto)reduced silver zeolites and attempts to distinguish between different luminescent species formed by autoreduction in zeolites and to correlate the emissive information with structural data.[26,33−40] For the first time, 2D excitation−emission graphs of silver clusters in zeolites are constructed to clearly identify the different emitters. Two major luminescence domains are observed corresponding to clusters capable of converting UV until blue light into green and red light, respectively. Depending on the framework type, the presence of specific cocations, and the degree of silver loading, the luminescent intensity and the spectral properties of the silver−zeolite materials can be tuned, in particular cases even outside the two major domains. In this way, a broad portfolio of bright fluorescent labels with emission colors spanning the whole visible range, including nearly white light generation, can be produced from cheap commercially available materials. The large Stokes shift is promising for applications as wavelength converters in, for example, fluorescence lamps and solar cells.

Experimental Methods

Synthesis of the Thermally Activated Silver-Exchanged Zeolite A Materials. Synthesis of the silver-exchanged zeolites was carried out starting from 500 mg of the zeolite material (K−A zeolite with Si/Al = 1; Na−A zeolite with Si/Al = 1; Ca−A zeolite with Si/Al = 1; Na−X zeolite with Si/Al = 1.3; Na−Y zeolite with Si/Al = 2.7; all samples are from Union Carbide). To allow an easy recognition of individual crystals in the fluorescence microscope, zeolite batches with micrometer-sized crystals were used (see Supporting Information for SEM pictures). The zeolite powder was suspended in 100 mL of MilliQ water containing the desired weight percentage of silver nitrate. A complete ion exchange occurred after being stirred in the dark for 2 h,[41] which was checked by the chloride precipitation method. The material was extensively washed with MilliQ water on a Büchner filter. The recovered white powder on top of the filter was gently heated (1−2°/min) under air to 450 °C for 1 day with 15-min stops at 50, 70, 90, 110, and 160 °C to avoid zeolite structure damage. The powder was allowed to cool to room temperature and was stored in the dark under dry atmosphere.

Large silver particles were not formed to a significant extent at the zeolite's outer surface by sintering of intrazeolite silver during the thermal treatment. The presence of such bulk silver should be reflected in the XRD patterns of the sample. Bulk silver has typical diffraction peaks at 2θ values of 38.1, 44.3, 64.4, and 77.5 corresponding to the (111), (200), (220), and (311) planes, respectively. The silver-exchanged sample did not show any significant difference with the blank sample (nonexchanged Na−A zeolite) at these positions (see XRD pattern in the Supporting Information); thus, the amount of larger silver nanoparticles was negligible. Even if larger silver aggregates would form locally, they would not contribute to the observed emission since such large particles are generally believed to be nonemissive although they may have a pronounced plasmon resonance light absorption band due to collective electron oscillations in the metal-like particles.

Nomenclature of the Heat-Treated Silver-Exchanged Zeolite Samples. The structural formulas for the A, X, and Y zeolites are, respectively, $(M^+_{12})[Si_{12}Al_{12}O_{48}]$, $(M^+_{10.4})[Si_{13.6}Al_{10.4}O_{48}]$, and $(M^+_{6.5})[Si_{17.5}Al_{6.5}O_{48}]$ after normalization of the total amount of T atoms in the unit cell to 24. The heat-treated silver-exchanged zeolite samples are further denoted by Ag_x,M−A, Ag_x,M−X, and Ag_x,M−Y, in which x represents the amount of silver atoms in the unit cell and M represents the cocation, being Na^+, K^+, or Ca^{2+}. The A, X, and Y zeolites are thus fully exchanged with silver for $x = 12$, 10.4, and 6.5, respectively.

Bulk Emission and Excitation Spectra of the Silver-Loaded Zeolites. The zeolite powder was sandwiched between a glass microscope slide and a quartz cover glass and sealed with

(16) Ozin, G. A.; Hugues, F. *J. Phys. Chem.* **1983**, *87*, 94.
(17) Seifert, R.; Rytz, R.; Calzaferri, G. *J. Phys. Chem. A* **2000**, *104*, 7473.
(18) Schulz-Ekloff, G. Metal Clusters in Zeolites. In *Comprehensive Supramolecular Chemistry*, 1st ed.; Alberti, B., Bein, T., Eds.; Pergamon: Oxford, 1996; Vol. 7; p 549.
(19) Baker, M. D.; Ozin, G. A.; Godber, J. *J. Phys. Chem.* **1985**, *89*, 305.
(20) Howard, J.; Waddington, T. C.; Wright, C. J. *J. Chem. Soc., Chem. Commun.* **1975**, 775.
(21) Jacobs, P. A.; Uytterhoeven, J. B.; Beyer, H. K. *J. Chem. Soc., Chem. Commun.* **1977**, 128.
(22) Ralek, M.; Grubner, O.; Beyer, H.; Jiru, P. *Collect. Czech. Chem. Commun.* **1962**, *27*, 142.
(23) Jacobs, P. A.; Tielen, M.; Linart, J.-P.; Uytterhoeven, J. B.; Beyer, H. *J. Chem. Soc., Faraday Trans.* **1976**, *72*, 2793.
(24) Seifert, R.; Kunzmann, A.; Calzaferri, G. *Angew. Chem., Int. Ed.* **1998**, *37*, 1522.
(25) Calzaferri, G.; Leiggener, C.; Glaus, S.; Schurch, D.; Kuge, K. *Chem. Soc. Rev.* **2003**, *32*, 29.
(26) Kim, Y.; Seff, K. *J. Am. Chem. Soc.* **1977**, *99*, 7055.
(27) Kim, Y.; Seff, K. *J. Am. Chem. Soc.* **1978**, *100*, 6989.
(28) De Cremer, G.; Antoku, Y.; Roeffaers, M. B. J.; Sliwa, M.; Van Noyen, J.; Smout, S.; Hofkens, J.; De Vos, D. E.; Sels, B. F.; Vosch, T. *Angew. Chem., Int. Ed.* **2008**, *47*, 2813.
(29) Michalik, J.; Kevan, L. *J. Am. Chem. Soc.* **1986**, *108*, 4247.
(30) Narayana, N.; Kevan, L. *J. Chem. Phys.* **1982**, *76*, 3999.
(31) Morton, J. R.; Preston, K. F. *J. Magn. Reson.* **1986**, *68*, 121.
(32) Peyser, L. A.; Vinson, A. E.; Bartko, A. P.; Dickson, R. M. *Science* **2001**, *291*, 103.
(33) Sun, T.; Seff, K. *Chem. Rev.* **1994**, *94*, 857.
(34) Beyer, H.; Jacobs, P. A. *Stud. Surf. Sci. Catal.* **1982**, *12*, 95.
(35) Gellens, L. R.; Mortier, W. J.; Lissillour, R.; Lebeuze, A. *J. Phys. Chem.* **1982**, *86*, 2509.
(36) Gellens, L. R.; Mortier, W. J.; Schoonheydt, R. A.; Uytterhoeven, J. B. *J. Phys. Chem.* **1981**, *85*, 2783.
(37) Gellens, L. R.; Mortier, W. J.; Uytterhoeven, J. B. *Zeolites* **1981**, *1*, 11.
(38) Grobet, P. J.; Schoonheydt, R. A. *Surf. Sci.* **1985**, *156*, 893.
(39) Kim, Y.; Seff, K. *J. Phys. Chem.* **1987**, *91*, 668.

tape. Emission spectra were taken at different excitation wavelengths from 260 to 680 nm with 20-nm intervals, using a Horiba Jobin Yvon Fluorolog fluorimeter. For every excitation wavelength, the emission was collected starting 20 nm above the excitation wavelength and ending at 800 nm. For excitation wavelengths below 420 nm, no emission was collected around the region where the emission wavelength equaled twice the excitation wavelengths, to avoid interference from second-order excitation peaks. The emission was detected in "front face mode" through the quartz cover glass. From the separate emission spectra at varying excitation wavelengths, the two-dimensional excitation−emission matrixes were constructed.

Single-Crystal Emission Spectra. As excitation source, the frequency-doubled output (375 or 400 nm, 8.18 MHz, 0.8 ps fwhm) of a mode-locked Ti:sapphire laser (Tsunami, Spectra Physics) was used. The excitation light, circularly polarized by use of a Berek polarization compensator (New Focus), was directed with a dichroic beam splitter into the oil-immersion objective (Olympus, 1.3 N.A., 100×) of an inverted microscope (Olympus IX70) equipped with a scanning stage (Physics Instruments). The excitation power was adjusted with a neutral density wheel at the entrance port of the microscope. The fluorescence was collected by the same objective, filtered (400- or 450-nm-long pass, Chroma Technology), split with a nonpolarizing beam splitter (50:50), and focused for one path onto an avalanche photodiode (SPCMAQ- 15, EG & G Electro Optics) to get scanning images. The other path was focused into a polychromator (Spectra Pro150 Acton Research Corporation) coupled to a back-illuminated liquid nitrogen-cooled CCD camera (LN/CCD-1340 × 400, Princeton Instruments) to record fluorescence spectra with a resolution down to 1 nm. To obtain spectra, the excitation power was adjusted to 10 until 100 W/cm^2 and an accumulation time between 1 and 10 s was used for the CCD camera. The obtained spectra were smoothed using a binomial filter.

Bulk Decay Measurements on the Nanosecond Time Scale. For the bulk nanosecond decay measurements at specific emission wavelengths, the same excitation source was used as for recording the single-crystal emission spectra. By using a Berek compensator (New Focus) in combination with a polarization filter, linearly polarized light was obtained, which was directed on the sample. This sample consisted of the zeolite powder pressed between a glass microscope slide and a quartz cover glass and was mounted under an angle of 45° with respect to the incident light. The emission was collected under 90° with respect to the incident light and guided through a polarization filter that was set at the magic angle (54.7°) with respect to the polarization of the excitation beam. Via a double monochromator (Sciencetech 9030, 6-nm bandwidth), the fluorescence was detected with a microchannel plate photomultiplier (MCP-PMT, R3809U, Hamamatsu) connected to a time-correlated single photon counting card (Becker & Hickl, SPC 830). The fluorescence decay analysis was performed with a homemade time-resolved fluorescence analysis (TRFA) software. The latter took pulse deconvolution into account, based on the Marquardt algorithm, and used a reweighted iterative reconvolution of the instrumental response function of the setup (about 50 ps) with a triexponential model function (M).[42] The decay contributions α were calculated from the decay times (τ) and their respective amplitudes (a):

$$\alpha_i = \frac{a_i \cdot \tau_i}{\sum_i a_i \cdot \tau_i} \quad (1)$$

Bulk Decay Measurements in the Microsecond Time Scale. For the time-resolved luminescence measurements, the 400-nm laser radiation was produced from a high-energy optical parametric oscillator (Newport MOPO series) pumped by a frequency-doubled Nd:YAG laser (Quanta-Ray PRO-Series, SpectraPhysics) at a repetition rate of 10 Hz. The laser pulse wavelength was 400 nm with a power of 30 mW. The luminescence of the powder sample, sandwiched between a glass microscope slide and a quartz cover glass and mounted under 45° with respect to the excitation beam, was detected at a right angle to the excitation beam with a high radiance monochromator (Applied Photophysics) coupled to a photomultiplier. The output of the photomultiplier (Hamamatsu R928) was fed into a digitizer (Tektronix TDS3000B Series) through an RC circuit with a characteristic time of 46.6 μs. A small fraction of the laser beam was reflected by a glass plate onto a photodiode (Newport 818-BB-21) to trigger the digitizer. Five hundred twelve signals were collected and averaged by the digitizer. The average signal was finally transferred to a PC to analyze the recorded data.

Single-Crystal Fluorescence Microscopy Pictures. Fluorescence microscope pictures of single emissive crystals were taken using an Olympus FluoView FV-500 inverted fluorescence microscope. The sample was excited by the light from a fluorescence mercury lamp. After passing a 320−380-nm band-pass filter, the excitation light was reflected on the sample by a 400-nm-long pass dichroic mirror. The emission light was collected and cleaned from excitation light by a 420-nm-long pass filter and detected with an RGB camera mounted on the front port. The dichroic mirror, as well as the long pass filter in the emission path, have a constant high transmission over the wavelength range from 450 to 800 nm, which guarantees that the color of the light reaching the detector is not influenced by the optics in the emission light path.

ESR Spectra. For measuring ESR spectra, the zeolite material was loaded into quartz tubes that were inserted in the double-rectangular TE_{104} cavity of the ESR spectrometer, which was cooled by liquid nitrogen to a temperature of 120 K. The spectra were taken on a Bruker 200D-SRC instrument in X-band with a sweep of 6800 T centered at 3450 T.

Results and Discussion

Thermal treatment of the silver-exchanged zeolite crystals at 450 °C produced colored powders with a spectrum ranging from yellow to deep red. Exposure to air immediately turns the samples white to yellowish again. The first color change has been ascribed to a temperature-induced dehydration of silver ions coordinating to the oxygen atoms of the zeolite lattice. In the dehydrated sample, a ligand-to-metal charge transfer from the zeolite lattice to the empty 5s orbital of the silver ion is responsible for the yellow color.[24] Upon rehydration, the absorption is strongly blue-shifted, resulting in a white-looking powder. While such ionic silver species are known to hardly fluoresce,[25] we observed bright luminescence under low-power UV excitation (Figure 1). Since cluster formation has been proven in silver-exchanged zeolites upon thermal treatment,[15] we ascribe the observed luminescence to oligoatomic silver clusters. Two plausible mechanisms can be proposed for the thermal autoreduction. The required electrons originate either from the framework-oxygen atoms that are expelled from the lattice[15] or from the oxidation of hydration water.[21] Since X-ray diffractograms of thermally treated silver zeolites (Supporting Information) show the typical diffraction pattern of an intact zeolite A structure, there is no significant lattice destruction. The second mechanism thus seems more plausible in this case. A typical TGA analysis on the silver-exchanged zeolites (Supporting Information) shows that even at temperatures up to 350 °C some hydration water is still left in the sample.

Upon closer examination of the luminescence of five different silver zeolite types under a narrow-line 360-nm UV excitation, we observed a broad range of colors and intensities depending

(40) Schoonheydt, R. A.; Leeman, H. *J. Phys. Chem.* **1989**, *93*, 2048.
(41) Sherry, H. S.; Walton, H. F. *J. Phys. Chem.* **1967**, *71*, 1457.
(42) Maus, M.; Cotlet, M.; Hofkens, J.; Gensch, T.; De Schryver, F. C.; Schaffer, J.; Seidel, C. A. M. *Anal. Chem.* **2001**, *73*, 2078.

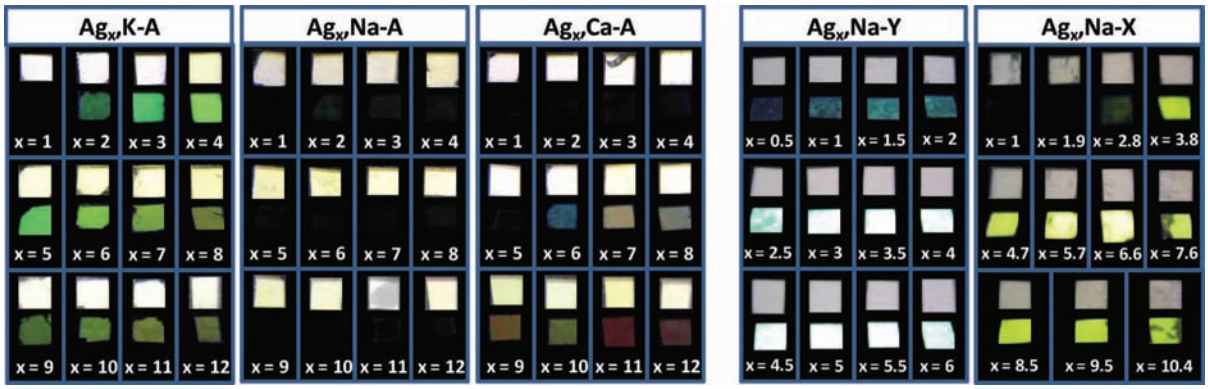

Figure 1. Photographs of silver-exchanged zeolites after heat treatment. The pictures are grouped per zeolite precursor (K−A, Na−A, Ca−A, Na−Y, and Na−X). For each silver loading, the upper picture represents the sample under room light illumination, while the lower picture is taken under UV illumination (360 nm).

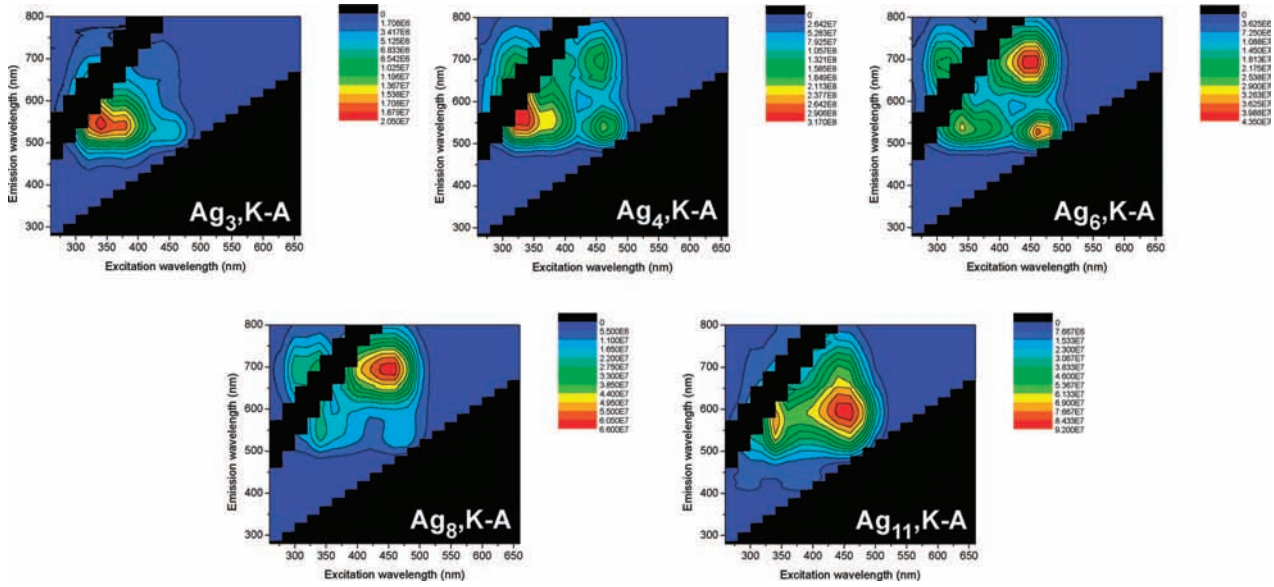

Figure 2. Representative 2D excitation−emission matrixes for heat-treated Ag$_x$,K−A zeolites.

on the zeolite topology, the presence of other counterions, and the degree of silver loadings (Figure 1). The Ag$_x$,K−A samples all give a yellow-greenish emission, while for Ag$_x$,Na−A hardly any fluorescence is observed at this excitation wavelength. For the Ag$_x$,Ca−A samples, the emission color strongly depends on the silver loading; higher silver loading results in a more red-shifted emission. The Ag$_x$,Na−Y samples show a bluelike emission that evolves to a remarkably bright white at higher silver loadings. The Ag$_x$,Na−X samples have a pronounced yellow emission with varying intensities.

The former analysis of the emissive behavior upon excitation by a narrow line gives a poorly detailed picture of the fluorescence properties of a material. To study the fluorescent properties of the silver-exchanged zeolites over the full wavelength range of excitation and emission, 2D excitation−emission matrixes are constructed by combining emission spectra taken at excitation wavelengths ranging from 260 to 600 nm with 20-nm intervals. In this way, the presence of different emitters in one sample is easily recognized.

A selection of the most representative graphs is given in Figures 2−5.[43] More 2D excitation−emission graphs are included in the Supporting Information. For clarity, the positions of the most intense luminescence bands for the different samples are summarized in Figure 6. As a control, the 2D excitation−emission graphs for the bare glass plate and a silver-free calcined Na−A zeolite were recorded (Supporting Information). While some background emission is observed for excitation below 300 nm, the intensity is several orders of magnitude lower than what is typically observed for thermally activated silver zeolites.

The Ag$_x$,K−A zeolite samples (Figure 2) with $x \leq 3$ show a major broad emission band between 530 and 580 nm with a corresponding excitation maximum of 330 ± 10 nm. For $4 \leq x \leq 6$, this band gradually disappears in favor of an excitation maximum at 450 ± 10 nm with the appearance of two emission bands at 530 ± 10 and 690 ± 10 nm. At higher loadings (x = 7−10), only the most red-shifted emitter is significant. At the highest silver loadings (x = 11 to 12), the emission is centered around 590 ± 10 nm upon excitation at 450 ± 10 nm.

The evolution of emitters at increasing silver loading for Ag$_x$,Na−A is somewhat different from that observed for Ag$_x$,K−A (Figure 3). At low silver loadings, the emitting species has a strong blue-shifted excitation spectrum (300 ± 10 nm) compared to the K^+ analogue with a high Stokes shift of about 330 nm. As the silver loading increases to x = 9, this band

(43) The absolute intensity scaling of one such graph is strongly dependent on the exact orientation and packing density of the sandwiched powder in the sample holder of the fluorimeter.

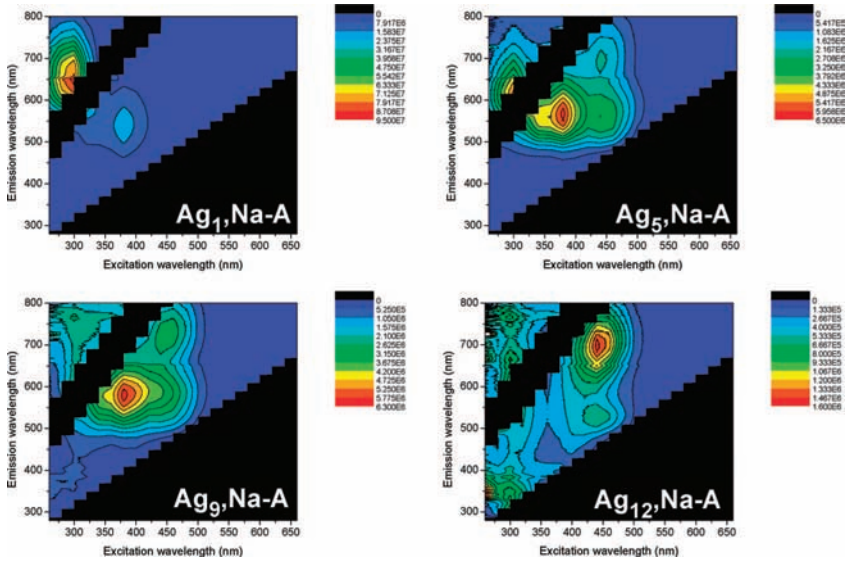

Figure 3. Representative 2D excitation−emission matrixes for heat-treated Ag_x,Na−A zeolites.

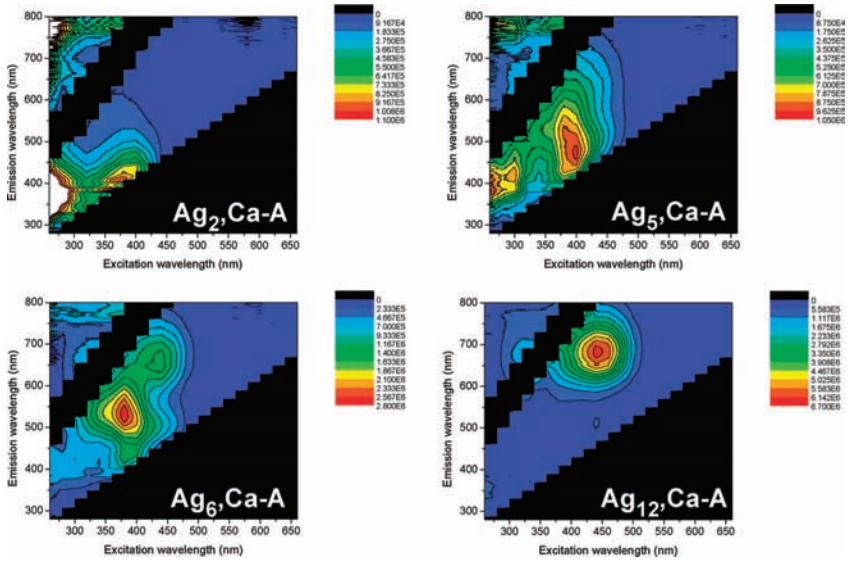

Figure 4. Representative 2D excitation−emission matrixes for heat-treated Ag_x,Ca−A zeolites.

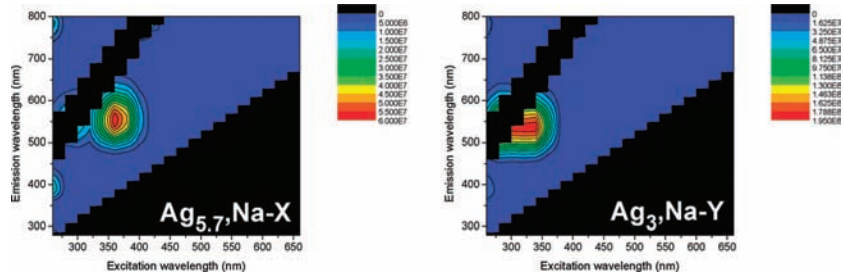

Figure 5. Representative 2D excitation−emission matrixes for heat-treated Ag_x,Na−X and Ag_x,Na−Y zeolites (both FAU topology).

gradually disappears in favor of a 560 ± 20 nm emitter excited at 380 ± 10 nm. A similar emitter was found in the K^+ samples. At the highest silver loadings, the 690-nm band, which was also found in the K^+ samples, becomes most pronounced.

When using zeolite A in its Ca^{2+} form as a starting material for silver exchange, the emissive properties at low silver loadings are different from the Na^+ samples, while at higher loadings they become similar to those of the Na^+ sample (Figure 4). For $x = 1-4$, the emission shows a lower Stokes shift (±40 nm) with an excitation centered around 360 nm. When $x = 5$, an intermediate emission domain is dominant, centered around 400 nm in excitation and 475 nm in emission. At $x = 6$, the typical 550-nm emitter from the K^+ and Na^+ samples is present and at higher loadings the red 690-nm emitter dominates.

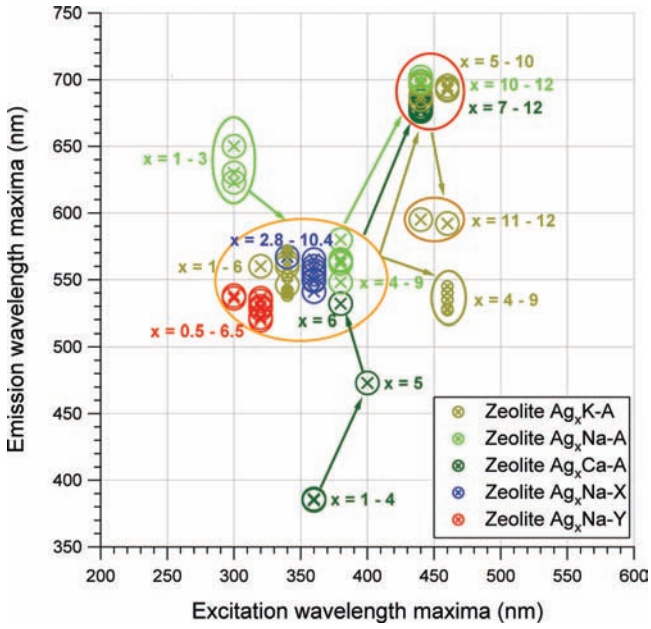

Figure 6. Position of the most pronounced luminescence bands of the heat-treated silver-exchanged zeolites. For each set of samples, the global trends upon increasing the silver loading are highlighted by the colored arrows. The resolution of the excitation maxima is 20 nm.

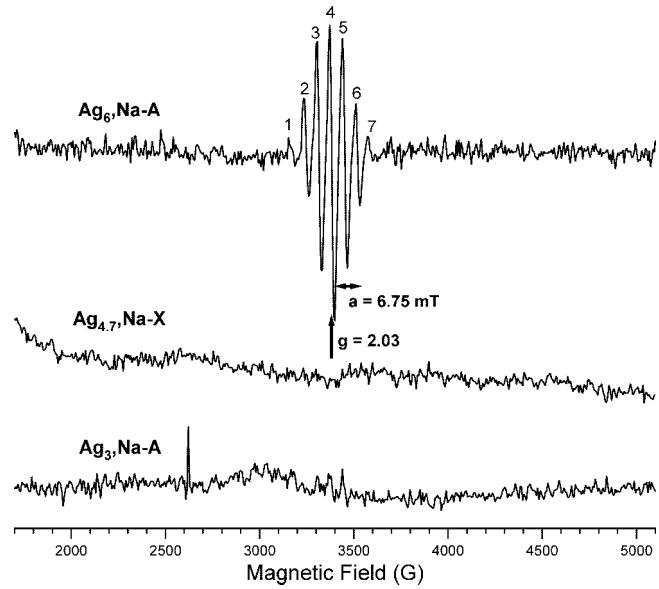

Figure 7. ESR spectra of silver-loaded zeolites. Upper: Representative spectrum for heat-treated Ag$_x$,Na−A zeolites with $x = 6-12$, showing the 690-nm emission. Middle and lower: ESR spectra of samples without 690-nm emission, the Ag$_{4.7}$,Na−X and Ag$_3$,Na−A zeolites, respectively. The spectra are corrected by subtracting the ESR spectrum of the corresponding silver-free zeolite material.

We thus demonstrated that the presence of cocations inside the zeolite strongly influences the clustering of the exchanged silver ions. This can be explained by differences in ion mobility, ion siting, cocation polarizability, and cocation size between the different coexchanged zeolite samples. In the specific case of the Ag$_x$,Ca−A samples, only half the amount of cocations (Ca^{2+}) are present compared to the corresponding Ag$_x$,K−A and Ag$_x$,Na−A samples. The influence of cocations on clustering of silver in zeolites has also been observed in an ESR study when reduction is carried out with hydrogen gas.[40]

Aside from the LTA topology, two FAU-type zeolites were also investigated with varying Si/Al ratios in their structure: Na−X with Si/Al = 1.3 and Na−Y with Si/Al = 2.7. The LTA and FAU topologies have a common building block: the sodalite cage.[44] Irrespective of the silver content, the silver clusters formed after thermal treatment in the FAU samples have an emission maximum around 540 ± 20 nm (Figure 5). The energy for excitation slightly shifts to lower wavelengths at increasing Si/Al ratios.

Thus, using our thermal procedure, at least seven different distinct emissive domains were recognized in LTA-type zeolites with two major recurring domains at 550- and 690-nm emission while in the FAU topology only the former emitter was identified. With the exception of some Ca−A samples with a low silver content, large Stokes shifts between 200 and 350 nm were observed, making these materials very interesting for the application as wavelength converters in, for example, fluorescence lamps or solar cells.

Structural information for silver clusters inside zeolites with intermediate to high silver loadings is available from X-ray analysis, ESR, and modeling studies.[14,26,29,30,33,35,36,40,45,46] As was also summarized by Sun and Seff,[33] there is wide agreement on the preferential formation and stabilization of triatomic (Ag_3^{n+}) and hexa-atomic (Ag_6^{n+}), more in particular Ag_6^{+} and Ag_6^{2+}, silver clusters in the sodalite cages. The exact cluster charges n are still a matter of debate. It is proposed that Ag_6^{2+} is formed by interaction of two Ag_3^{+} clusters, eventually followed by a reduction to Ag_6^{+}.[29,33] While in LTA-type zeolites both clusters have been observed, there is no clear evidence in literature for the presence of Ag_6^{n+} in FAU. It has been proposed that, after formation of a triatomic cluster in the sodalite cages of FAU zeolites, further clustering is inhibited.[21,33,47]

Our fluorescence-based observations seem to match these structural findings: two major silver cluster species were identified (550- and 690-nm emitters) for the LTA samples, while only the 550-nm emitter was observed in the FAU samples. It thus seems logical that the reported Ag_3^{n+} and Ag_6^{n+} clusters correspond to, respectively, the 550- and 690-nm emitters. To find evidence for this statement, we investigated our samples with ESR spectroscopy. Some representative ESR spectra of heat-treated silver zeolites are presented in Figure 7. For highly loaded silver Na−A zeolites ($x \geq 6$) where the 600-nm emitter is present, a clear seven-line signal around $g = 2.03$ with a hyperfine splitting constant a of 6.75 mT is observed. Although the two outer peaks of this signal are rather small, it can be clearly distinguished from a five-line signal based on the intensity ratios between the peaks (Supporting Information). Samples lacking 690-nm emission, such as the yellow-emitting Ag$_{4.7}$,Na−X and the Ag$_3$,Na−A zeolites, are ESR-silent (Figure 7, middle and lower spectra).

The hyperfine splitting of the ESR signal into seven lines for the 690-nm emitting samples results from coupling of the electron spin with six equivalent nuclear spins ($I = {}^1/_2$). Therefore, this signal is attributed to a hexameric Ag_6^{n+} (with $n = 1$, 3, or 5) cluster. The g-value of 2.03 as well as the

(44) International Zeolite Association. http://www.iza-online.org.
(45) Texter, J.; Kellerman, R.; Gonsiorowski, T. *J. Chem. Phys.* **1986**, *85*, 637.
(46) Texter, J.; Kellerman, R.; Gonsiorowski, T. *J. Phys. Chem.* **1986**, *90*, 2118.
(47) Grosse, R.; Burmeister, R.; Boddenberg, B.; Gedeon, A.; Fraissard, J. *J. Phys. Chem.* **1991**, *95*, 2443.

hyperfine splitting constant (a = 6.75 mT) are in perfect agreement with values earlier reported for Ag_6^+ clusters in zeolites.[29,40,48] The isotope effect of ^{107}Ag and ^{109}Ag cannot be resolved because of the small coupling constant compared to the rather large line width. The charge of Ag_6^{n+} (n = 1, 3, or 5) cannot be extracted directly from the ESR analysis, although most reports agree on a monovalent Ag_6^+ cluster.[33,40,49]

Similar ESR lines from hexameric silver clusters were obtained for other samples (e.g., Ag_{12},Ca−A) as expected from the presence of the 690-nm emitter in the fluorescence spectra (Figure 6). The absence of the 690-nm band in the fluorescence data for, for example, the heat-treated Ag_3,Na−A and $Ag_{4.7}$,Na−X (Figure 7; middle and lower spectra) is in agreement with the ESR-silent nature of these samples. Although the appearance of the 690-nm emitter is associated with the ESR signal of a hexameric silver cluster with a doublet electronic ground state, probably Ag_6^+, it cannot be excluded that the observed emission originates from the ESR-silent Ag_6^{2+}, whose occurrence is reported to be associated with the Ag_6^+ cluster formation in LTA zeolites. The bright yellow-emitting cluster present in LTA samples with lower silver loading and in FAU samples is EPR-silent and thus has a singlet electronic ground state. As most of the literature reports on the presence of a trimeric silver cluster in zeolites with low to intermediate silver loadings, the emission likely originates from a Ag_3^+ cluster.

As seen in the overview of Figure 6, other emitters are also present in specific samples. As ESR analyses are sensitive only toward selected cluster types, this technique is unable to provide structural information for all these species. Extensive X-ray studies with Rietveld refinement in combination with theoretical modeling may be helpful also to identify these other emitters.

Luminescence decay analysis of the 550-nm emitters in the LTA frameworks, assigned to Ag_3^+ clusters with singlet ground state, revealed a multiexponential decay in the nanosecond time scale, indicative for spin-allowed transitions (Figure 8). An exponential decay with three components was necessary to adequately fit the data, yielding typically a fast (<0.5 ns), an intermediate (1.0−2.5 ns), and a slower (3.5−6.5 ns) decay component with varying contributions. The presence of three decay components indicates the 550-nm emitter is present in at least three different local environments (for instance, with different degrees of quenching).

A different picture is seen for the hexameric silver cluster cluster, emitting around 690 nm. The Ag_8,Ca−A sample is taken as a reference sample for this cluster, based on its 2D excitation−emission graph that shows only one intensity peak in this region (Figure 4 and Supporting Information). The luminescence decay is dominated by two slow components of 115 μs (42.5%) and 835 μs (57.5%) (Figure 9); thus, spin-forbidden intersystem crossing is probably occurring here, being a singlet−triplet transition in the case of a Ag_6^{2+} cluster or a doublet−quadruplet transition in the case of Ag_6^+. Similar long luminescence decay times were also found in other types of silver−zeolite systems.[50]

To localize the origin of luminescence within a single particle, fluorescence microscopy images of individual crystals were recorded, as depicted in Figure 10a for Ag_6,K−A. A homogeneous distribution of emission over the full individual crystal is observed. As the outer rims are not brighter than the inner surface, the clusters seem homogeneously distributed over the whole crystal.

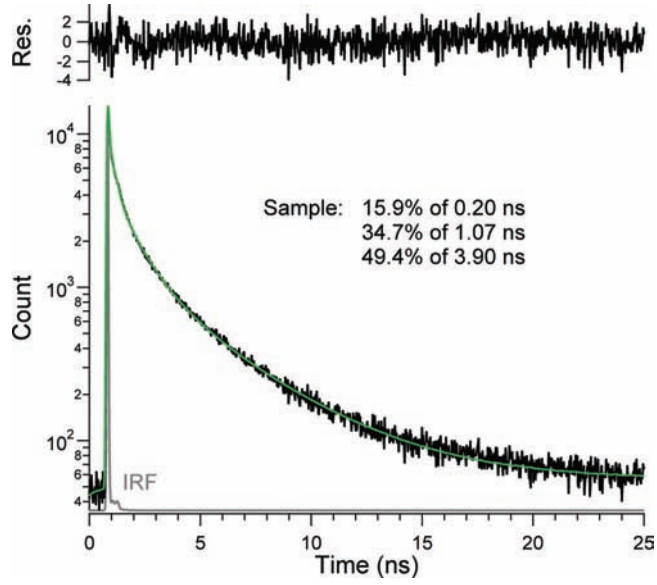

Figure 8. Nanosecond decay of the luminescence at 550 nm from a heat-treated Ag_6,Na−A zeolite sample upon 375-nm picosecond-pulsed excitation. The green curve represents a triexponential fit to the experimental data (black curve), based on an algorithm that takes deconvolution with the instrumental response function (gray curve) into account.

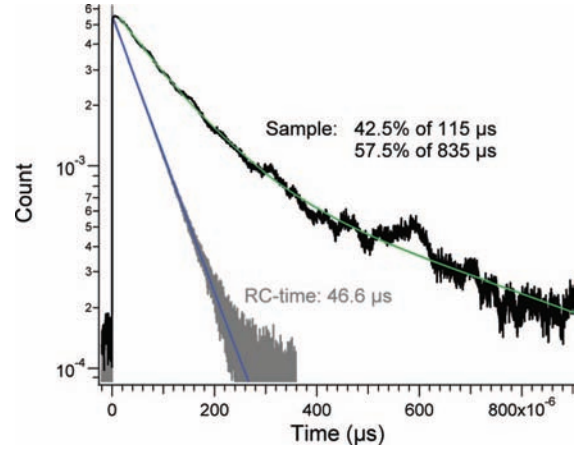

Figure 9. Microsecond decay of the luminescence from a heat-treated Ag_8,Ca−A zeolite sample upon 400-nm excitation. The green curve represents a two-exponential fit to the experimental data (black curve). Two slow decay components could be resolved: a 115- and 835-μs component with relative amplitudes of 42.5 and 57.5%, respectively. The blue line shows the monoexponential fit to a decay obtained by a scattering solution (gray curve) to determine the characteristic time of the RC circuit.

Figure 10b shows the normalized emission spectra upon 400-nm illumination for individual Ag_6,Na−A crystals (colored curves), exciting preferably the Ag_3^+. The black curve corresponds to the normalized emission recorded with a fluorimeter for the bulk powder. Many of the colored curves nicely follow the black "ensemble averaged" spectrum with an emission maximum at about 570 nm, whereas only a few individual crystals show an emission spectrum that is slightly blue-shifted up to 40 nm. These slight heterogeneities are characteristic for zeolite materials. In other single-crystal studies, the properties

(48) Hermerschmidt, D.; Haul, R. *Ber. Bunsen-Ges. Phys. Chem.* **1980**, *84*, 902.
(49) Michalik, J.; Sadlo, J.; Kodaira, T.; Shimomura, S.; Yamada, H. *J. Radioanal. Nucl. Chem.* **1998**, *232*, 135.
(50) Bruhwiler, D.; Leiggener, C.; Glaus, S.; Calzaferri, G. *J. Phys. Chem. B* **2002**, *106*, 3770.

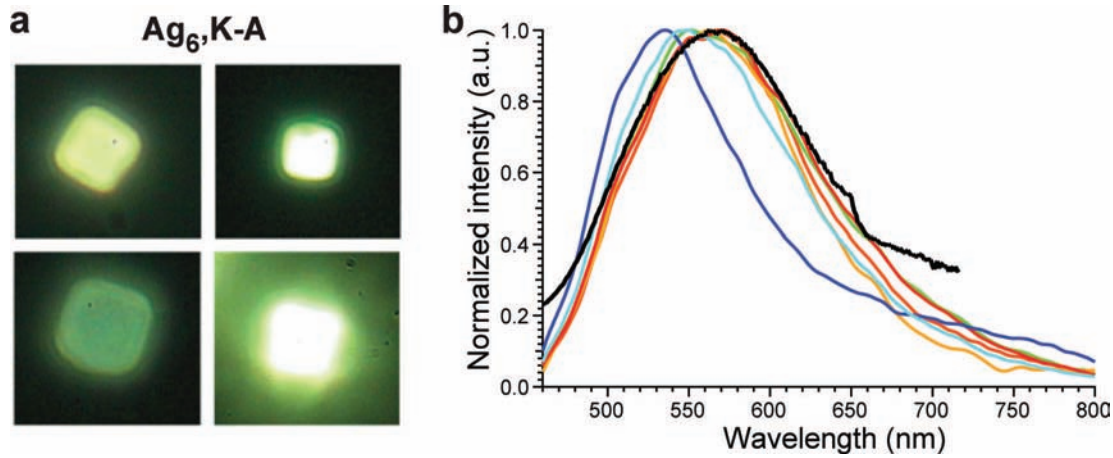

Figure 10. Single-crystal emission characterization for the Ag_3^+ clusters inside zeolite A. (a) True-color fluorescence microscopy images of four individual heat-treated Ag_6,K−A zeolite crystals upon UV excitation. It is clear that the emission is not restricted to the outer rim of the crystal. The emission can thus be assigned to intraporous silver clusters. The individual crystals have sizes ranging from 2 to 5 μm. (b) Emission spectra of Ag_6,Na−A zeolites upon 400-nm illumination. The black curve corresponds to the bulk spectrum (measured in a fluorimeter), while the colored curves represent spectra from individual crystals measured on a confocal fluorescence microscope.

of the individual crystals from one synthesis batch were also found to show heterogeneities.[51−55]

Conclusions

We described a convenient route for the creation of stable oligoatomic (partially) reduced silver clusters within zeolite matrixes by a simple ion-exchange process followed by thermal treatment. These clusters have interesting emissive properties that may find numerous applications, for instance, as wavelength converters in fluorescence lamps or solar cells, or as bright and photostable biocompatible labels. Depending on the zeolite topology, the presence of specific counterions, and the silver loading, different emissive species are created upon thermal treatment, with spectral properties ranging from blue- to red-emitting species. In most cases at intermediate silver loadings, a yellow fluorescent band around 550 nm is observed with likely a Ag_3^+ cluster as representative species, while for LTA zeolites at higher loadings a possible candidate species emitting around 690 nm is formed. Interestingly, the luminescence of the 690-nm emitter decays slowly over a few hundred microseconds, which is interpreted in terms of a spin-forbidden doublet−quadruplet transition in case of a Ag_6^+ cluster. A detailed spectroscopic characterization at the single-crystal level revealed a small degree of heterogeneity among different crystallites from one synthesis batch.

Acknowledgment. T.V., M.B.J.R., and G.D.C. acknowledge the Fonds voor Wetenschappelijk Onderzoek (FWO) for two postdoctoral fellowships and a doctoral fellowship, respectively. This work was performed within the framework of the IAP-VI Program Supramolecular Chemistry and Catalysis of the Belgian federal government and GOA-2/01. We also gratefully acknowledge financial support from the Flemish Ministry of Education (ZWAP 04/007) and from K.U. Leuven in the frame of the Centre of Excellence CECAT, of "Industrieel onderzoeksfonds" (IOF/07/HB023) and "Bijzonder onderzoeksfonds" (BOF; IDO-project). Peter Lievens, Sabina Wyczawska, and Pieterjan Claes are acknowledged for the alignment of the Nd:YAG laser and the OPO system. Thanks to Lars Giebeler for help with the XRD measurements.

Supporting Information Available: A short overview of the used zeolite frameworks, SEM pictures, additional 2D excitation−emission graphs of heat-treated silver zeolites, XRD and TGA analyses, and more details on the treatment of the ESR spectra. This material is available free of charge via the Internet at http://pubs.acs.org.

JA810071S

(51) Hashimoto, S.; Yamashita, S. *ChemPhysChem* **2004**, *5*, 1585.
(52) Roeffaers, M. B. J.; Sels, B. F.; Uji-i, H.; Blanpain, B.; L'Hoest, P.; Jacobs, P. A.; De Schryver, F. C.; Hofkens, J.; De Vos, D. E. *Angew. Chem., Int. Ed.* **2007**, *46*, 1706.
(53) Roeffaers, M. B. J.; De Cremer, G.; Uji-i, H.; Muls, B.; Sels, B. F.; Jacobs, P. A.; De Schryver, F. C.; De Vos, D. E.; Hofkens, J. *Proc. Natl. Acad. Sci. U.S.A.* **2007**, *104*, 12603.
(54) Roeffaers, M. B. J.; Hofkens, J.; De Cremer, G.; De Schryver, F. C.; Jacobs, P. A.; De Vos, D. E.; Sels, B. E. *Catal. Today* **2007**, *126*, 44.
(55) Roeffaers, M. B. J.; Ameloot, R.; Baruah, M.; Uji-i, H.; Bulut, M.; De Cremer, G.; Muller, U.; Jacobs, P. A.; Hofkens, J.; Sels, B. F.; De Vos, D. E. *J. Am. Chem. Soc.* **2008**, *130*, 5763.